



Does stress transmission in forelands depend on structural style? Distinctive stress magnitudes during Sevier thin-skinned and Laramide thick-skinned layer-parallel shortening in the Bighorn Basin (USA) revealed by stylolite and calcite twinning paleopiezometry

Nicolas Beaudoin¹ | Olivier Lacombe² | Marie-Eléonore David² | Daniel Koehn³

¹Université de Pau et des Pays de l'Adour, E2S UPPA, CNRS, TOTAL, LFCR, Pau, France

²Sorbonne Université, CNRS-INSU, Institut des Sciences de la Terre de Paris, Paris, France

³GeoZentrum Nordbayern, University Erlangen-Nuremberg, Erlangen, Germany

Correspondence

Nicolas Beaudoin, Université de Pau et des Pays de l'Adour, E2S UPPA, CNRS, TOTAL, LFCR, Pau, France.
Email: nicolas.beaudoin@univ-pau.fr

Funding information

Sorbonne Université, Grant/Award Number: C14313; European Union Seventh Framework Programme for research, technological development and demonstration, Grant/Award Number: n°316889

Abstract

The Sheep Mountain-Little Sheep Mountain Anticlines, Bighorn Basin (USA) formed as basement-cored Laramide structures in the formerly undeformed foreland of the thin-skinned Sevier orogen. We take advantage of the well-constrained microstructural network there to reconstruct differential stress magnitudes that prevailed during both Sevier and Laramide layer-parallel shortening (LPS), before the onset of large-scale folding. Differential stress magnitudes determined from tectonic stylolites are compared and combined to previous stress estimates from calcite twinning paleopiezometry in the same formations. During stress loading related to LPS, differential stress magnitudes transmitted from the distant Sevier thin-skinned orogen into the sedimentary cover of the Bighorn basin (11–43 MPa) are higher than the differential stress magnitudes accompanying the early stage of LPS related to the thick-skinned Laramide deformation (2–19 MPa). This study illustrates that the tectonic style of an orogen affects the transmission of early orogenic stress into the stable continental interior.

1 | INTRODUCTION

Providing quantitative estimates of the evolution of past stress magnitudes over time is a challenging task, albeit important to understand the long-term mechanical and paleohydrological behaviour of the upper crust. While strain mostly distribute at plate boundaries, there is a significant intraplate stress transmission thousands of kilometres away from the source of the stress that leads to the development of mesostructures such as fractures or stylolites before and/or beyond macrostructures such as folds and thrusts (Lacombe & Mouthereau, 1999; Tavani et al., 2015; Weil & Yonkee, 2012). The use of calcite twinning paleopiezometry documented an overall cratonward decrease in orogenic stress, with a drop of differential stress ($\sigma_d = \sigma_1 - \sigma_3$) values in the first hundred kilometres from the orogen hinterland/foreland boundary

(>100 MPa to 20 MPa; Beaudoin & Lacombe, 2018). The reason of this stress transmission pattern and its dependence on the orogenic tectonic style are still debated (Lacombe, 2010; Van der Pluijm, Craddock, Graham, & Harris, 1997). To tackle this issue, we combined existing stress data from calcite twinning paleopiezometry (Amrouch, Lacombe, Bellahsen, Daniel, & Callot, 2010) with original σ_d values obtained from stylolite roughness paleopiezometry (Ebner, Toussaint, Schmittbuhl, Koehn, & Bons, 2010; Schmittbuhl, Renard, Gratier, & Toussaint, 2004) from the sedimentary cover of the Sheep Mountain-Little Sheep Mountain anticlines (Bighorn Basin, Wyoming, USA; Figure 1) where the network of systematic veins/mesoscale faults and paleostress reconstructions document two stages of layer-parallel shortening (LPS), related to thin-skinned (i.e. basement remaining undeformed) then to thick-skinned (i.e. involving the basement) tectonics.

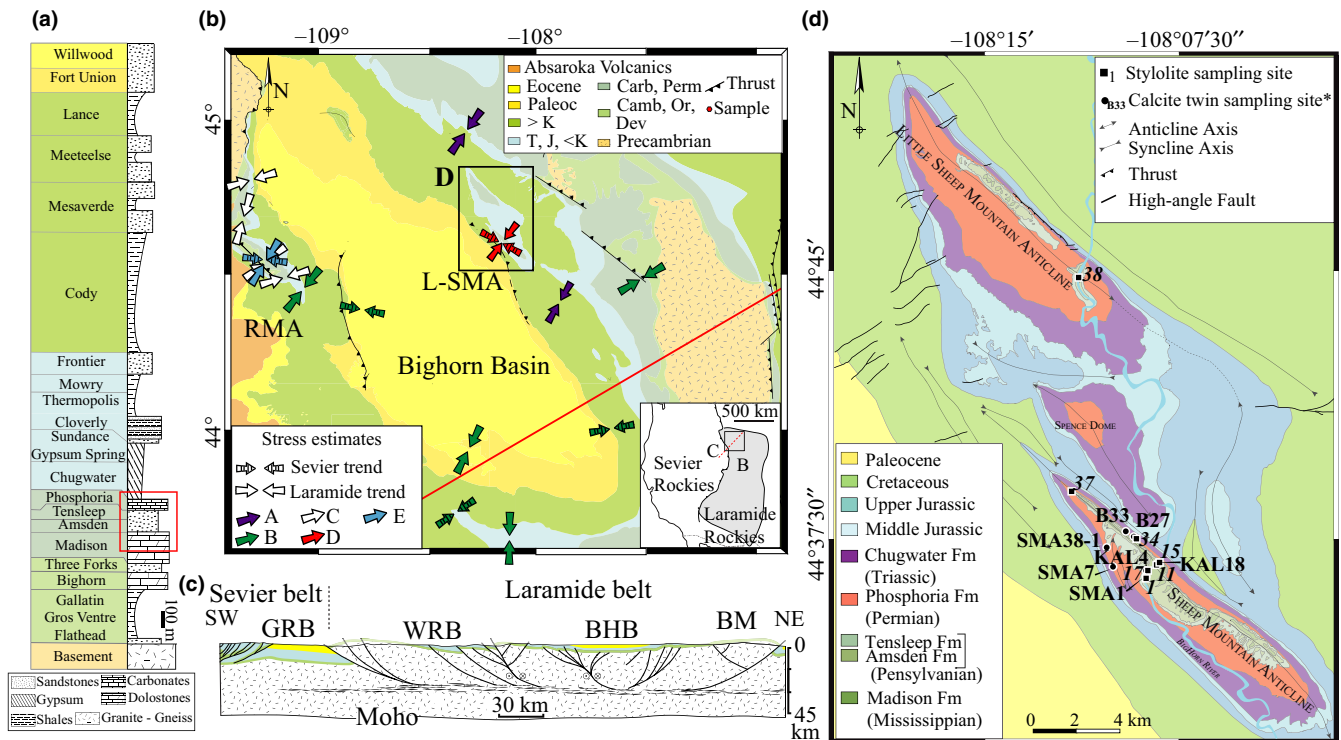


FIGURE 1 (a) Stratigraphic column of the Bighorn Basin, modified after Neely and Erslev (2009). Red frames correspond to the studied formations, colours are related to the age of the formations following the key presented in B. (b) Geological map of the Bighorn Basin (Wyoming, USA), the insert shows the location of the area with regard to simplified tectonic provinces, it also shows the location of the map B as a black frame and of the cross-section C as a red line. The reconstructed orientations of the horizontal maximum principal stress are reported as plain arrows for the Laramide event, and as crossed arrows for the Sevier event. Orientations are from A: Varga (1993), B: Craddock and Van der Pluijm (1999), C: Neely and Erslev (2009), D: Amrouch et al. (2010), E: Beaudoin et al. (2012). (c) Cross section modified after Marshak et al. (2000). (d) Simplified geological maps of the Little Sheep Mountain-Sheep Mountain anticline. Location of sampling sites for tectonic stylolite paleopiezometry and for calcite twinning paleopiezometry are reported as numbered squares and labelled circles, respectively (* from Amrouch et al., 2010) [Colour figure can be viewed at wileyonlinelibrary.com]

2 | GEOLOGICAL SETTING

The Bighorn Basin belongs to the thick-skinned Laramide Province of the Rocky Mountains (Figure 1c) that formed by latest Cretaceous until Paleogene times in response to the flat-slab subduction of the Farallon plate (Yonkee & Weil, 2015). Micro/meso-structural studies combined with absolute dating of vein cements (Amrouch et al., 2010; Beaudoin, Bellahsen, Lacombe, Emmanuel, & Pironon, 2014; Beaudoin, Lacombe, Roberts, & Koehn, 2018; Beaudoin et al., 2012; Bellahsen, Fiore, & Pollard, 2006a; Craddock & van der Pluijm, 1999; Neely & Erslev, 2009; Varga, 1993; Weil & Yonkee, 2012; Yonkee & Weil, 2010) show that the sedimentary strata of the Bighorn Basin recorded (a) pre-Laramide LPS, related to compressive stress likely transmitted from the distant thin-skinned Sevier orogen at the time the basin was still part of the Sevier undeformed foreland (vein set S, σ_1 striking WNW-ESE prior to folding, 81–72 Ma, Figure 2a); (b) Laramide LPS (vein set L-1, σ_1 striking NE-SW prior to folding, 72–50 Ma, Figure 2a); (c) Laramide thrust-related, basement-cored folding with veins developed at fold hinges (vein Set L-2, 50–35 Ma, Figure 2a). Field observations also document the occurrence of bed perpendicular tectonic stylolites with peaks oriented (a) ~WNW-ESE and (b) NE-SW after unfolding (Figure 2b, 2c; Amrouch, Beaudoin,

Lacombe, Bellahsen, & Daniel, 2011; Amrouch et al., 2010). The orientations of the stylolite peaks, commonly considered as reliable markers of the orientation of the tectonic stress (e.g. Koehn, Renard, Toussaint, & Passchier, 2007; Tavani et al., 2015; Weil & Yonkee, 2012), together with their kinematic compatibility and chronological relationships with the veins of set S and L-1, respectively (Figure 2c), and with the conjugate reverse and strike-slip mesoscale faults that also developed during Laramide LPS (Amrouch et al., 2011, 2010) unambiguously support that these tectonic stylolites witness the successive horizontal compressive stress related to the Sevier and Laramide events, respectively.

3 | STYLOLITE ROUGHNESS INVERSION FOR STRESS

Stylolites are serrated surfaces (Figure 2b) that develop by chemical dissolution under stress (Alvarez, Engelder, & Geiser, 1978; Fletcher & Pollard, 1981; Koehn et al., 2007; Toussaint et al., 2018). The growth and the morphology of a stylolite are rate-dependent (e.g. Stockdale, 1922); they are governed by the kinetics of dissolution and the distribution of heterogeneities, and are affected by the amount of clay enhancing the

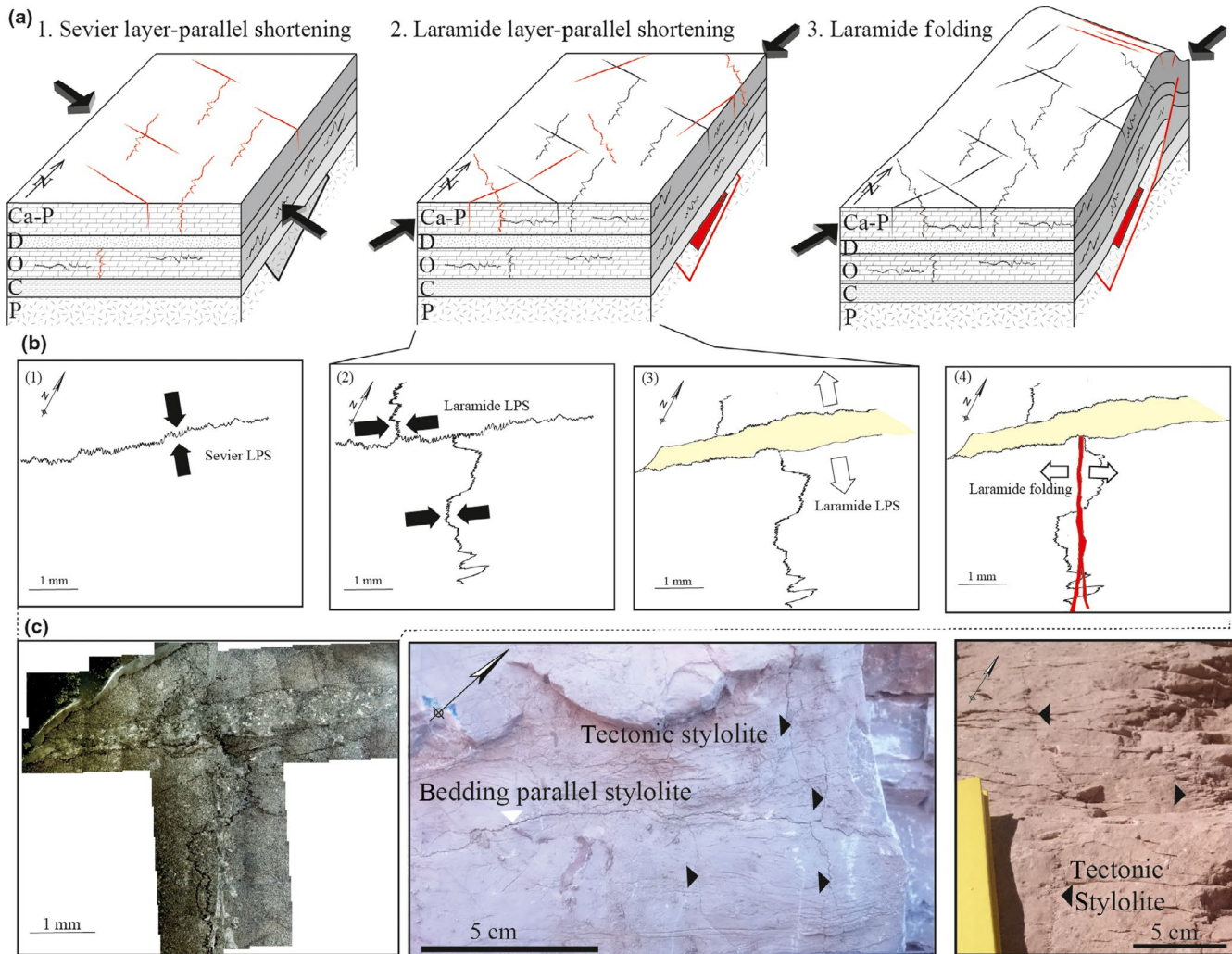


FIGURE 2 (a) Schematic diagrams reporting the compressional trend, mode I veins (sets S, L-1, L-2), and stylolites developed during the Sevier LPS (1), the Laramide LPS (2) and the Laramide folding (3). The pre-existing structures are reported in black, the developing ones in red. For the sake of clarity, we omitted the Triassic-Paleogene overlying strata. P: Precambrian basement, C: Cambrian, O: Ordovician, D: Devonian, Ca-P: Carboniferous and Permian. (b) Sketch of microstructural observations proposing a possible sequence between tectonic stylolites with peaks oriented (1) WNW-ESE and (2) NE-SW and between veins oriented (3) NE-SW and (4) NW-SE, based on observed abutment and reopening relationships and supported by the general Sevier-Laramide sequence of deformation. (c) On the left-hand side, microphotograph of the thin section on which sequence B was built. On the right-hand side, field photographs of tectonic and bedding parallel stylolites in the Madison Formation at Sheep Mountain Anticline [Colour figure can be viewed at wileyonlinelibrary.com]

dissolution (Renard, Dysthe, Feder, Bjørlykke, & Jamtveit, 2001). Once dissolution starts, there is a thermodynamic competition between (a) a destabilizing (roughening) force due to pinning particles on the stylolite surface that resist dissolution, and (b) stabilizing (smoothing) forces, long-range elastic forces and local surface tension, that tend to flatten the stylolite surface by preferentially dissolving areas of local roughness (Schmittbuhl et al., 2004). While the topography of the stylolite during its growth is sensitive to both strain rate and stress (Koehn, Ebner, Renard, Toussaint, & Passchier, 2012), the final topography of a stylolite is a saturation state that is reached over a short period of time, ca. 200 years (Schmittbuhl et al., 2004) at the end of dissolution due to local drop in solubility (Rolland et al., 2012). Hence, the final roughness, that is, the difference in height between two points along the stylolite plane, reflects the ambient stress at the time pressure-dissolution

stopped, and is dependent on neither strain rate nor lithology (Ebner, Koehn, Toussaint, Renard, & Schmittbuhl, 2009).

The stress inversion technique relies upon a fractal analysis of high-resolution 2D scans (12,800 dpi) of the final roughness on the stylolite surface. In most cases, the 1D topography of a stylolite is best described by a self-affine scaling invariance (Schmittbuhl et al., 2004), that is, the rough shape is invariant under a range of scales. A classic way to determine the self-affinity of a signal is to analyze it with a Fourier power spectrum, that relates the wave number k (mm^{-1}) to the squared Fourier transform modulus $P(k)$ as $P(k) \propto k^{2H+1}$, where H is the roughness (or Hurst) exponent (Barabási & Stanley, 1995). In the case of stylolites, such analysis typically exhibits 2 power laws (Figure 3a): a large-scale (usually > 1 mm) law with a specific roughness exponent of 1.1 which reflects the elastic energy

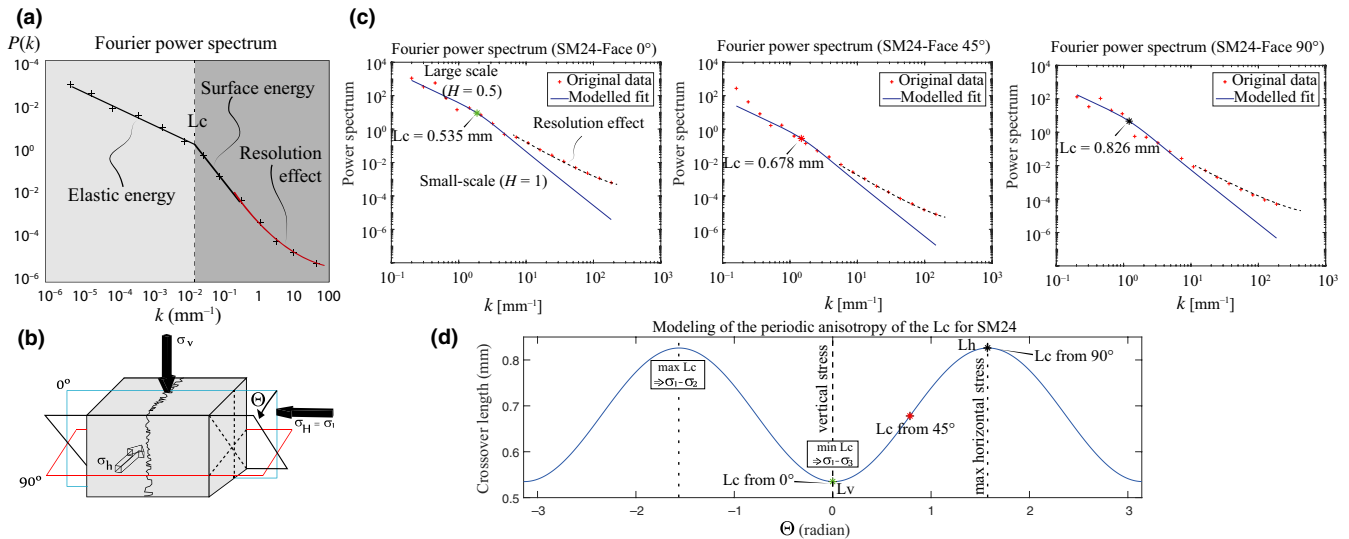


FIGURE 3 (a) Ideal example of Fourier power spectrum applied to 1D profile of stylolite roughness, showing the different expected power laws and where the crossover length sits. (b) Sketch of the cuttings through a tectonic stylolite to access the stylolite-plane anisotropy (after Beaudoin et al., 2016). (c) Example of treatment for three cuts on the sample SM24, crossover lengths L_c are reported as coloured crosses within 23% uncertainty. (d) Reconstructed periodic anisotropy of the L_c for the Sample SM24, using the L_c and angles presented in C. Similar dataset are presented for all samples as Figures S1–S3 [Colour figure can be viewed at wileyonlinelibrary.com]

dominated regime; and a small-scale law with a specific roughness exponent of 0.5 which reflects the surface energy dominated regime. A third part of the data forms a flat tail at the lowest scales that reflects a resolution effect related to image treatment (Figure 3a). The scale of observation at which the self-affine invariance switches from one power law to the other one, defined as the crossover length L_c , is directly linked to the absolute magnitude of the mean and differential stresses (σ_m and σ_d , respectively) that prevailed at the end of the life of a stylolite as $L_c = \frac{\gamma E}{\beta \sigma_m \sigma_d}$, with E the Young's modulus (Pa), γ the solid–fluid interfacial energy (J.m⁻²) and β a dimensionless constant $\beta = \nu(1-2\nu)/\pi$ with ν being the Poisson's ratio (Schmittbuhl et al., 2004).

The evolution of the topography and related L_c on tectonic stylolite surfaces exhibits a periodic anisotropy of the L_c (Ebner, Toussaint, et al., 2010) that can be reconstructed from a minimum of three cuts normal to the surface if one knows the mechanical/chemical parameters of the dissolved rock (Figure 3b; Beaudoin et al., 2016). If the reconstructed anisotropy returns minima and maxima aligned with the vertical and horizontal directions (Figure 3d), then it provides access to the horizontal crossover length L_h and to the vertical crossover length L_v , which yield the magnitudes of the horizontal maximum (σ_H) and minimum (σ_h) stresses as $\frac{L_h}{L_v} = \frac{\sigma_H - \sigma_v}{\sigma_H - \sigma_h}$, provided the vertical stress σ_v (i.e. the weight of overburden) is known (Ebner, Toussaint, et al., 2010).

4 | SAMPLING STRATEGY AND RESULTS

Because stylolite occurrence depends on lithology (Marshak & Engelder, 1985) and to limit the variability of rock type and

mechanical properties of samples, Sevier and Laramide-related tectonic stylolites were collected at different structural locations solely in the partly dolomitized, grainstone facies of the Mississippian Madison Formation and of the Permian Phosphoria Formation (Barbier, Hamon, Callot, Floquet, & Daniel, 2012; Figure 1a).

Three peak-parallel cuts were done for each stylolite with an angle between each cut (Table 1), and each roughness signal was inverted using the Fourier power spectrum (Figure 3c) (Ebner, Piazzolo, Renard, & Koehn, 2010; Renard, 2004). The L_c anisotropy was reconstructed from the three values of L_c (Figure 3d) (Beaudoin et al., 2016). Successful inversion comprises 13 tectonic stylolites (Table 1, Figures S1–S3) sampled in the Madison Formation ($n = 10$) and in the Phosphoria Formation ($n = 3$).

To determine σ_d values, we considered a range of depths of deformation obtained by comparing published basin models (Beaudoin, Lacombe, Bellahsen, Amrouch, & Daniel, 2014; May et al., 2013) with the range of absolute U–Pb ages of the systematic veins S and L-1 related to Sevier and Laramide LPS (Beaudoin et al., 2018). This reveals that the Madison Formation was buried at depths of 1500–2450 m and 2450–2800 m at the time of Sevier and Laramide LPS, respectively (and we consider an average of 300 m less for the Phosphoria Fm.). We also use Poisson ratio and Young modulus obtained from mechanical tests on the Phosphoria and Madison Formations from Sheep Mountain (Amrouch et al., 2011, Table 1) and the classic solid–fluid interfacial energy value for dolomite (0.24 J.m⁻², Wright, Cygan, & Slater, 2001). The L_c is estimated assuming a linear-by-parts fit of the Fourier spectra modelled by a least square algorithm (Ebner et al., 2009). Such analytical solution returns the L_c within a 23% uncertainty (Rolland, Toussaint, Baud, Conil, & Landrein, 2014) that can be considered as the maximum methodological uncertainty as other parameters are known. Note

TABLE 1 Location of samples and results of inversion of tectonic stylolite roughness for stress in the Little Sheep Mountain–Sheep Mountain anticlines, USA

Sample name and location		Teeth				Anisotropy of Lc ^b				Principal stress magnitude (MPa)			Average Differential Stress (MPa)		
Name	GPS	Longitude	Latitude	Formation	Bedding	Orientation ^a	Angle of cut (°)	Lc from FPS ^b (mm)	Lv	Lh	Depth ^c (m)	σ_1	σ_2	σ_3	Stress Ratio
Little Sheep Mountain Anticline															
LSM-S6	38	-108.19008	44.741	Madison	horizontal	N120	0	0.968	0.968	0.163	1,500	nan	35	nan	24
							50	0.504			2,450	62	58	38	0.17
							90	0.163							
LSM-S13	38	-108.19008	44.741	Madison	horizontal	N105	0	0.643	0.28	0.57	1,500	52	44	35	14
							90	0.471			2,450	69	63	58	0.55
							140	0.287							
LSM-S11	38	-108.19008	44.741	Madison	horizontal	N042	0	0.394	0.36	0.64	2,450	67	62	58	8.5
							15	0.368			2,800	74	70	66	0.5
							90	0.619							
LSM-S16	38	-108.19008	44.741	Madison	horizontal	N045	0	0.231	0.15	0.74	2,450	78	73	58	19
							90	0.666			2,800	84	80	66	0.22
							75	0.535							
Sheep Mountain Anticline															
SM-S1	1	-108.13924	44.606	Madison	068–16S	N110	0	0.401	0.38	0.84	1,500	48	42	35	11
							60	0.649			2,450	67	63	58	0.44
							90	0.829							
SM-S22-1	15	-108.13253	44.615	Madison	120–64N	N113	0	0.725	0.27	1.56	1,500	52	49	35	14.5
							45	0.294			2,450	70	67	58	0.25
							90	1.025							
SM-S22-2	15	-108.13253	44.615	Madison	120–64N	N130	0	0.424	0.42	0.59	1,500	52	49	35	14.5
							90	0.59			2,450	70	67	58	0.25
							125	0.537							
SM-S31	37	-108.19825	44.649	Phosphoria	125–36W	N140	0	0.397	0.37	0.78	1,250	50	40	29	17.5
							60	0.591			2,250	67	60	53	0.5
							90	0.726							
SM-S18	11	-108.13253	44.615	Madison	145–47E	N040	0	0.3	0.22	0.52	2,450	73	66	58	14
							90	0.493			2,800	79	74	66	0.38
							120	0.515							
SM-S10	17	-108.14007	44.611	Madison	113–17S	N045	0	1.996	1.62	4.36	2,450	60	59	58	2
							45	2.451			2,800	68	67	66	0.5
							90	4							

(Continues)

TABLE 1 (Continued)

Sample name and location				Teeth Orientation ^a	Angle of cut (°)	Lc from FPS ^b (mm)	Anisotropy of Lc ^b		Principal stress magnitude (MPa)			Average Differential Stress (MPa)	Stress Ratio		
Name	GPS Longitude	Latitude	Formation				Bedding	N045	0	Lv	Lh			Depth ^c (m)	σ_1
SM-S24	34	-108.14711	44.622	Phosphoria	120-76S	N045	0	0.535	0.826	2,300	66	57	54	11.5	0.75
SM-S32	37	-108.19825	44.649	Phosphoria	125-36W	N045	0	0.902	1.826	2,600	66	63	61	5.5	0.6
SM-S22-3	15	-108.13253	44.615	Madison	125-59E	N045	0	1.294	0.458	2,450	61	58	53	7	0.38
							55	0.735		2,800	67	66	61		0.17
							90	0.458							

Note: Vertical principal stress is reported in bold. horizontal principal stresses are calculated considering for the Phosphoria ($E = 41$ Gpa, $\nu = 0.25$, $\mu = 0.24$ J/m²) and for the Madison ($E = 29$ Gpa, $\nu = 0.2$; $\mu = 0.24$ J/m²).

^aorientation after correction from local bedding attitude.

^bCrossover length Lc given within 23% of uncertainty.

^cRange of depth considered based on burial model (see text for details).

that an extra source of uncertainties can be found in the modelling of the periodic anisotropy from three cuts (Beaudoin et al., 2016).

Laramide-related σ_d values ($n = 8$) range from 2 ± 0.5 MPa to 19 ± 4.4 MPa ($n = 7$) while Sevier-related σ_d values ($n = 5$) range from 11 ± 2.2 MPa to 24 ± 4.8 MPa ($n = 6$).

5 | DISCUSSION AND CONCLUSIONS

σ_d estimates from inversion of the roughness of tectonic stylolites were compared with published σ_d estimates from calcite twinning paleopiezometry in the same formations (Figure 4) (Amrouch et al., 2010). We discarded the published σ_d values from calcite twinning paleopiezometry interpreted as reflecting local stress perturbations at the tip of the upward propagating Laramide thrust (Amrouch et al., 2010; Bellahsen, Fiore, & Pollard, 2006b) rather than the regional stress field of interest.

To account for the fact σ_d values inferred from tectonic stylolites are systematically lower than those inferred from calcite twinning when considering each deformation event (i.e. Sevier or Laramide) (Figure 4), we propose that stylolite development mostly predates vein formation and calcite twinning strain in a stress build-up model. This sequence could be the reason why the local stress perturbation above the tip of the basement fault is

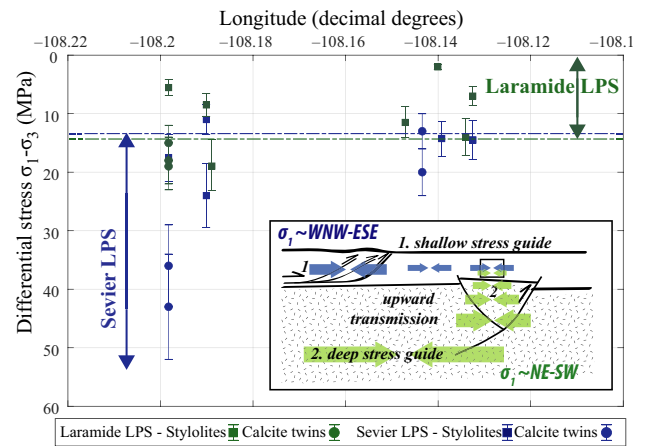


FIGURE 4 Location of samples (according to their longitude in decimal degrees) versus differential stress magnitudes ($\sigma_1 - \sigma_3$, MPa) obtained from inversion of tectonic stylolite roughness (squares) and calcite twinning (circles). Green data points represent the Laramide-related σ_d , and the blue data points represent the Sevier-related σ_d . Error bars on squares account for the overall uncertainty for each method. Double arrows and dashed lines represent the range of σ_d exclusive to Laramide layer-parallel shortening (green) and to Sevier layer-parallel shortening (blue), considering uncertainties. Insert is a conceptual model of stress transmission through shallow and deep stress guides that accounts for the difference in σ_d magnitudes sustained by sedimentary cover rocks during thin-skinned Sevier and thick-skinned Laramide LPS. Compressive stress related to Sevier (1) and Laramide (2) layer-parallel shortening is reported as blue and green convergent arrows, respectively, with larger size reflecting qualitatively higher σ_d . LPS - Layer Parallel Shortening [Colour figure can be viewed at wileyonlinelibrary.com]

not recorded by the tectonic stylolites. We propose that during stress build-up in the flat-lying strata, pressure solution initiated with low σ_d along planar solubility heterogeneities in rocks (such as elongated pores) and halted rapidly, presumably by clogging around the dissolution planes (Toussaint et al., 2018). Stylolites would have therefore dissipated the earliest part of the stress build-up before saturating. Then, because increasing stress would not have been accommodated fully by pressure solution, stress would have accumulated enough to trigger vein development and calcite twinning, until newly formed mesoscale faulting ultimately took place if the required σ_d was reached.

Integration of both paleopiezometers highlights that most σ_d values related to Sevier LPS (11 ± 2.2 – 43 ± 9 MPa) are notably higher than σ_d values (2 ± 0.5 – 19 ± 4 MPa) related to Laramide LPS. The results document for the first time a systematic difference in σ_d magnitudes sustained by flat-lying strata at the same place in relation to the evolving deformation style over time. The σ_d values derived from both paleopiezometers reflect the σ_d prevailing at the burial depth at which the strata underwent LPS. Because the depth of deformation of strata was larger during the Laramide LPS than during the Sevier LPS ($\Delta_{\text{depth}} \sim 650$ m on average, Table 1) and since σ_d increases with depth (Beaudoin & Lacombe, 2018; Lacombe, 2007), the normalization to a similar depth simply increases the difference between σ_d values associated with the Sevier and the Laramide LPS, thus confirming that this difference in σ_d values reflects a significant trend.

We propose that the stress recorded in the Bighorn Basin was first efficiently transmitted from the distant Sevier thin-skinned orogen into the stable foreland through a shallow stress guide, that is the sedimentary cover (Figure 4), where the stress reached values compatible with the σ_d values derived from calcite twins for the Sevier foreland elsewhere (20–40 MPa, van der Pluijm et al., 1997). We further propose that the low Laramide σ_d reconstructed in the cover rocks represents only a fraction of the source stress transmitted forelandward through a deep (crustal or lithospheric) stress guide (Figure 4) (Erslev, 1993). We speculate that most of the stress was dissipated at depth while triggering the inversion of inherited basement normal faults (Lacombe & Bellahsen, 2016; Marshak, Karlstrom, & Timmons, 2000) and so as it was transmitted upward into the attached cover during the early stage of Laramide LPS, ~ 20 Ma after the onset of exhumation of Laramide basement arches (Beaudoin, Lacombe, Roberts, & Koehn, 2019), the Laramide LPS-related σ_d remained much lower compared to former Sevier σ_d values. It was only at the time of later generalized Laramide large-scale basement-cored folding that σ_d strongly increased to reach their maximum values in the cover rocks (Amrouch et al., 2011).

This study therefore illustrates that the tectonic style of an orogen affects the magnitude of the σ_d transmitted towards the stable continental interior and therefore challenges previous models of cratonward decrease in σ_d regardless of the structural style of the orogen. Beyond regional implications, this study further establishes tectonic stylolite roughness inversion as a reliable and powerful paleopiezometer to constrain stress build-up in poorly deformed strata

of stable orogenic forelands, which places it as a useful complement of calcite twinning paleopiezometry.

ACKNOWLEDGEMENTS

This work was funded by Sorbonne Université (research agreement C14313) and by the European Union Seventh Framework Programme for research, technological development and demonstration (grant agreement n°316889). NB is funded through the ISITE program E2S, supported by ANR PIA and Région Nouvelle-Aquitaine. Authors thank Stephen Marshak, Adolf Yonkee, Atilla Aydin and two anonymous reviewers for their constructive comments that greatly improved the manuscript, as well as the science editor Jean Braun.

DATA AVAILABILITY STATEMENT

The data that support the findings of this study are provided in the supplementary material.

ORCID

Nicolas Beaudoin  <https://orcid.org/0000-0002-7027-8599>

Olivier Lacombe  <https://orcid.org/0000-0003-4167-7344>

Daniel Koehn  <https://orcid.org/0000-0002-2276-2626>

REFERENCES

- Alvarez, W., Engelder, T., & Geiser, P. A. (1978). Classification of solution cleavage in pelagic limestones. *Geology*, 6(5), 263–266. [https://doi.org/10.1130/0091-7613\(1978\)6<263:COSCIIP>2.0.CO;2](https://doi.org/10.1130/0091-7613(1978)6<263:COSCIIP>2.0.CO;2)
- Amrouch, K., Beaudoin, N., Lacombe, O., Bellahsen, N., & Daniel, J.-M. (2011). Paleostress magnitudes in folded sedimentary rocks. *Geophysical Research Letters*, 38(17), L17301. <https://doi.org/10.1029/2011GL048649>
- Amrouch, K., Lacombe, O., Bellahsen, N., Daniel, J.-M., & Callot, J.-P. (2010). Stress and strain patterns, kinematics and deformation mechanisms in a basement-cored anticline: Sheep Mountain Anticline, Wyoming. *Tectonics*, 29(1), TC1005. <https://doi.org/10.1029/2009TC002525>
- Barabási, A., & Stanley, H. (1995). In A. Barabási, & H. Stanley (Eds.), *Fractal Concepts in Surface Growth* (p. 366). Cambridge: Cambridge University Press.
- Barbier, M., Hamon, Y., Callot, J.-P., Floquet, M., & Daniel, J.-M. (2012). Sedimentary and diagenetic controls on the multiscale fracturing pattern of a carbonate reservoir: The Madison Formation (Sheep Mountain, Wyoming, USA). *Marine and Petroleum Geology*, 29, 50–67. <https://doi.org/10.1016/j.marpetgeo.2011.08.009>
- Beaudoin, N., Bellahsen, N., Lacombe, O., Emmanuel, L., & Pironon, J. (2014). Crustal-scale fluid flow during the tectonic evolution of the Bighorn Basin (Wyoming, USA). *Basin Research*, 26(3), 403–435. <https://doi.org/10.1111/bre.12032>
- Beaudoin, N., Koehn, D., Lacombe, O., Lecouty, A., Billi, A., Aharonov, E., & Parlangeau, C. (2016). Fingerprinting stress: Stylolite and calcite twinning paleopiezometry revealing the complexity of progressive stress patterns during folding-The case of the Monte Nero anticline in the Apennines, Italy. *Tectonics*, 35(7), 1687–1712. <https://doi.org/10.1002/2016TC004128>
- Beaudoin, N., & Lacombe, O. (2018). Recent and future trends in paleopiezometry in the diagenetic domain: Insights into the tectonic paleostress and burial depth history of fold-and-thrust belts and sedimentary basins. *Journal of Structural Geology*, 114, 357–365. <https://doi.org/10.1016/j.jsg.2018.04.001>

- Beaudoin, N., Lacombe, O., Bellahsen, N., Amrouch, K., & Daniel, J.-M. (2014). Evolution of pore-fluid pressure during folding and basin contraction in overpressured reservoirs: Insights from the Madison-Phosphoria carbonate formations in the Bighorn Basin (Wyoming, USA). *Marine and Petroleum Geology*, 55, 214–229. <https://doi.org/10.1016/j.marpetgeo.2013.12.009>
- Beaudoin, N., Lacombe, O., Roberts, N. M. W., & Koehn, D. (2018). U-Pb dating of calcite veins reveals complex stress evolution and thrust sequence in the Bighorn Basin, Wyoming, USA. *Geology*, 46(11), 1015–1018. <https://doi.org/10.1130/G45379.1>
- Beaudoin, N., Lacombe, O., Roberts, N. M. W., & Koehn, D. (2019). U-Pb dating of calcite veins reveals complex stress evolution and thrust sequence in the Bighorn Basin, Wyoming, USA: REPLY. *Geology*, 47(9), e481–e481. <https://doi.org/10.1130/G46606Y.1>
- Beaudoin, N., Leprêtre, R., Bellahsen, N., Lacombe, O., Amrouch, K., Callot, J.-P., ... Daniel, J.-M. (2012). Structural and microstructural evolution of the Rattlesnake Mountain Anticline (Wyoming, USA): New insights into the Sevier and Laramide orogenic stress build-up in the Bighorn Basin. *Tectonophysics*, 576–577, 20–45. <https://doi.org/10.1016/j.tecto.2012.03.036>
- Bellahsen, N., Fiore, P., & Pollard, D. D. (2006a). The role of fractures in the structural interpretation of Sheep Mountain Anticline, Wyoming. *Journal of Structural Geology*, 28(5), 850–867. <https://doi.org/10.1016/j.jsg.2006.01.013>
- Bellahsen, N., Fiore, P. E., & Pollard, D. D. (2006b). From spatial variation of fracture patterns to fold kinematics: A geomechanical approach. *Geophysical Research Letters*, 33(2). <https://doi.org/10.1029/2005GL024189>
- Craddock, J. P., & van der Pluijm, B. A. (1999). Sevier-Laramide deformation of the continental interior from calcite twinning analysis, west-central North America. *Tectonophysics*, 305, 275–286. [https://doi.org/10.1016/S0040-1951\(99\)00008-6](https://doi.org/10.1016/S0040-1951(99)00008-6)
- Ebner, M., Koehn, D., Toussaint, R., Renard, F., & Schmittbuhl, J. (2009). Stress sensitivity of stylolite morphology. *Earth and Planetary Science Letters*, 277(3–4), 394–398. <https://doi.org/10.1016/j.epsl.2008.11.001>
- Ebner, M., Piazzolo, S., Renard, F., & Koehn, D. (2010). Stylolite interfaces and surrounding matrix material: Nature and role of heterogeneities in roughness and microstructural development. *Journal of Structural Geology*, 32(8), 1070–1084. <https://doi.org/10.1016/j.jsg.2010.06.014>
- Ebner, M., Toussaint, R., Schmittbuhl, J., Koehn, D., & Bons, P. (2010). Anisotropic scaling of tectonic stylolites: A fossilized signature of the stress field? *Journal of Geophysical Research*, 115(B6), B06403. <https://doi.org/10.1029/2009JB006649>
- Erslev, E. A. (1993). Thrusts, back-thrusts, and detachment of Rocky Mountain foreland arches. *Geological Society of America Special Paper*, 280, 339–358.
- Fletcher, R. C., & Pollard, D. D. (1981). Anticrack model for pressure solution surfaces. *Geology*, 9, 419–424. [https://doi.org/10.1130/0091-7613\(1981\)9<419:AMFPSS>2.0.CO;2](https://doi.org/10.1130/0091-7613(1981)9<419:AMFPSS>2.0.CO;2)
- Koehn, D., Ebner, M., Renard, F., Toussaint, R., & Passchier, C. W. (2012). Modelling of stylolite geometries and stress scaling. *Earth and Planetary Science Letters*, 341–344, 104–113. <https://doi.org/10.1016/j.epsl.2012.04.046>
- Koehn, D., Renard, F., Toussaint, R., & Passchier, C. (2007). Growth of stylolite teeth patterns depending on normal stress and finite compaction. *Earth and Planetary Science Letters*, 257(3–4), 582–595. <https://doi.org/10.1016/j.epsl.2007.03.015>
- Lacombe, O. (2007). Comparison of paleostress magnitudes from calcite twins with contemporary stress magnitudes and frictional sliding criteria in the continental crust: Mechanical implications. *Journal of Structural Geology*, 29(1), 86–99. <https://doi.org/10.1016/j.jsg.2006.08.009>
- Lacombe, O. (2010). Calcite twins, a tool for tectonic studies in thrust belts and stable orogenic forelands. *Oil & Gas Science and Technology—revue d'IFP Energies Nouvelles*, 65(6), 809–838. <https://doi.org/10.2516/ogst/2009088>
- Lacombe, O., & Bellahsen, N. (2016). Thick-skinned tectonics and basement-involved fold-thrust belts: Insights from selected Cenozoic orogens. *Geological Magazine*, 153(5–6), 763–810. <https://doi.org/10.1017/S0016756816000078>
- Lacombe, O., & Mouthereau, F. (1999). What is the real front of orogens? The Pyrenean orogen as a case study. *Comptes Rendus De L Academie Des Sciences Serie II Fascicule A-Sciences De La Terre Et Des Planetes*, 329, II, 889–896.
- Marshak, S., & Engelder, T. (1985). Development of cleavage in limestones of a fold-thrust belt in eastern New York. *Journal of Structural Geology*, 7(3–4), 345–359. [https://doi.org/10.1016/0191-8141\(85\)90040-9](https://doi.org/10.1016/0191-8141(85)90040-9)
- Marshak, S., Karlstrom, K., & Timmons, J. M. (2000). Inversion of Proterozoic extensional faults: An explanation for the pattern of Laramide and Ancestral Rockies intracratonic deformation. *United States: Geology*, 28(8), 735–738. [https://doi.org/10.1130/0091-7613\(2000\)028<0735:IOPEFA>2.3.CO;2](https://doi.org/10.1130/0091-7613(2000)028<0735:IOPEFA>2.3.CO;2)
- May, S. R., Gray, G. G., Summa, L. L., Stewart, N. R., Gehrels, G. E., & Pecha, M. E. (2013). Detrital zircon geochronology from the Bighorn Basin, Wyoming, USA: Implications for tectonostratigraphic evolution and paleogeography. *Geological Society of America Bulletin*, 125(9–10), 1403–1422. <https://doi.org/10.1130/B30824.1>
- Neely, T. G., & Erslev, E. A. (2009). The interplay of fold mechanisms and basement weaknesses at the transition between Laramide basement-involved arches, north-central Wyoming, USA. *Journal of Structural Geology*, 31(9), 1012–1027. <https://doi.org/10.1016/j.jsg.2009.03.008>
- Renard, F. (2004). Three-dimensional roughness of stylolites in limestones. *Journal of Geophysical Research*, 109(B3), B03209. <https://doi.org/10.1029/2003JB002555>
- Renard, F., Dysthe, D., Feder, J., Bjørlykke, K., & Jamtveit, B. (2001). Enhanced pressure solution creep rates induced by clay particles: Experimental evidence in salt aggregates. *Geophysical Research Letters*, 28(7), 1295–1298. <https://doi.org/10.1029/2000GL012394>
- Rolland, A., Toussaint, R., Baud, P., Conil, N., & Landrein, P. (2014). Morphological analysis of stylolites for paleostress estimation in limestones. *International Journal of Rock Mechanics and Mining Sciences*, 67, 212–225. <https://doi.org/10.1016/j.ijrmms.2013.08.021>
- Rolland, A., Toussaint, R., Baud, P., Schmittbuhl, J., Conil, N., Koehn, D., ... Gratier, J.-P. (2012). Modeling the growth of stylolites in sedimentary rocks. *Journal of Geophysical Research: Solid Earth*, 117(B6), B06403. <https://doi.org/10.1029/2011JB009065>
- Schmittbuhl, J., Renard, F., Gratier, J. P., & Toussaint, R. (2004). Roughness of stylolites: Implications of 3D high resolution topography measurements. *Physical Review Letters*, 93(23), 238501. <https://doi.org/10.1103/PhysRevLett.93.238501>
- Stockdale, P. B. (1922). *Stylolites: Their nature and origin-PhD* (p. 97). Indiana University.
- Tavani, S., Storti, F., Lacombe, O., Corradetti, A., Muñoz, J. A., & Mazzoli, S. (2015). A review of deformation pattern templates in foreland basin systems and fold-and-thrust belts: Implications for the state of stress in the frontal regions of thrust wedges. *Earth-Science Reviews*, 141, 82–104.
- Toussaint, R., Aharonov, E., Koehn, D., Gratier, J. P., Ebner, M., Baud, P., ... Renard, F. (2018). Stylolites: A review. *Journal of Structural Geology*, 114, 163–195. <https://doi.org/10.1016/j.jsg.2018.05.003>
- van der Pluijm, B. A., Craddock, J. P., Graham, B. R., & Harris, J. H. (1997). Paleostress in Cratonic North America: Implications for Deformation of Continental Interiors. *Science*, 277, 794–796. <https://doi.org/10.1126/science.277.5327.794>
- Varga, R. J. (1993). Rocky Mountain foreland uplifts: Products of a rotating stress field or strain partitioning? *Geology*, 21(12), 1115–1119.

[https://doi.org/10.1130/0091-7613\(1993\)021<1115:RMFUPO>2.3.CO;2](https://doi.org/10.1130/0091-7613(1993)021<1115:RMFUPO>2.3.CO;2)

- Weil, A. B., & Yonkee, W. A. (2012). Layer-parallel shortening across the Sevier fold-thrust belt and Laramide foreland of Wyoming: Spatial and temporal evolution of a complex geodynamic system. *Earth and Planetary Science Letters*, 357-358, 405-420. <https://doi.org/10.1016/j.epsl.2012.09.021>
- Wright, K., Cygan, R. T., & Slater, B. (2001). Structure of the (1014) surfaces of calcite, dolomite and magnesite under wet and dry conditions. *Physical Chemistry Chemical Physics*, 3, 839-844.
- Yonkee, W. A., & Weil, A. B. (2010). Reconstructing the kinematic evolution of curved mountain belts: Internal strain patterns in the Wyoming salient, Sevier thrust belt, U.S.A. *Geological Society of America Bulletin*, 122(1-2), 24-49. <https://doi.org/10.1130/B26484.1>
- Yonkee, W. A., & Weil, A. B. (2015). Tectonic evolution of the Sevier and Laramide belts within the North American Cordillera orogenic system. *Earth-Science Reviews*, 150, 531-593. <https://doi.org/10.1016/j.earscirev.2015.08.001>

SUPPORTING INFORMATION

Additional supporting information may be found online in the Supporting Information section.

Figure S1. Results of stylolite roughness inversion, per sample in the Little Sheep Mountain anticline. A- Crossover lengths L_c are reported as crosses within 23% uncertainty for the three cuts, B- Reconstructed periodic anisotropy for the corresponding samples,

red squares are L_c , dotted line represents the vertical plane with respect to the orientation of the stylolite before strata tilting.

Figure S2. Results of stylolite roughness inversion, per sample in the Sheep Mountain anticline. Crossover lengths L_c are reported as crosses within 23% uncertainty for the three cuts, B- Reconstructed periodic anisotropy for the corresponding samples, red squares are L_c , dotted line represents the vertical plane with respect to orientation of the stylolite before strata tilting.

Figure S3. Results of stylolite roughness inversion, per sample in the Sheep Mountain anticline. Reconstructed periodic anisotropy for the corresponding samples presented on Figure S2, red squares are L_c , dotted line represents the vertical plane with respect to orientation of the stylolite before strata tilting.

How to cite this article: Beaudoin N, Lacombe O, David M-E, Koehn D. Does stress transmission in forelands depend on structural style? Distinctive stress magnitudes during Sevier thin-skinned and Laramide thick-skinned layer-parallel shortening in the Bighorn Basin (USA) revealed by stylolite and calcite twinning paleopiezometry. *Terra Nova*. 2020;32:225-233. <https://doi.org/10.1111/ter.12451>